First-principles calculation of defect-formation energies in the $Y_2(Ti,Sn,Zr)_2O_7$ pyrochlore

Wendy R. Panero* and Lars Stixrude
Department of Geological Sciences, University of Michigan, Ann Arbor, Michigan 48109-1063, USA

Rodney C. Ewing
Department of Geological Sciences, Department of Materials Science and Engineering, Department of Nuclear Engineering and Radiological Sciences, University of Michigan, Ann Arbor, Michigan 48109-1063, USA

(Received 13 January 2004; revised manuscript received 3 June 2004; published 30 August 2004)

Isometric pyrochlore, $A_2B_2O_7$, with compositions in the $Y_2(Ti,Sn,Zr)_2O_7$ ternary system, are of particular interest because there are dramatic changes in properties, such as ionic conductivity, and response to radiation damage, as a function of disordering of the A- and B-site cations and oxygen vacancies. First-principles calculations using density functional theory and the plane-wave pseudopotential method, predict lattice constants (1.0049–1.0463 nm), atomic coordinates, and bulk moduli (176–205 GPa) that are linearly dependent on the B-site cation radius (0.062–0.072 nm). However, the energetics for the formation of cation-antisite (0–2 eV) and Frenkel-pair (4–11 eV) defects do not correlate with cation size, underscoring the importance of the specific electronic configuration of the B-site cation. The greater degree of covalent bonding between $\langle Sn^{4+}\text{-}O\rangle$ as compared with $\langle Ti^{4+}\text{-}O\rangle$ or $\langle Zr^{4+}\text{-}O\rangle$ results in defect formation energies otherwise unexpected solely due to the radius ratios of the cation species. $Y_2Sn_2O_7$ shows 2–4 eV greater defect formation energies than otherwise predicted through mean B-site cation sizes. Relaxed calculations on coupled cation-antisite and Frenkel-pair defects show that cation-antisite reactions likely drive the oxygen-Frenkel pair defect formation process that ultimately leads to increased oxygen mobility and completely aperiodic structures. Total charge and partial density of states calculations show strikingly different behavior of oxygen on two different crystallographic positions, emphasizing the need for a full account of the electronic structure.

DOI: 10.1103/PhysRevB.70.054110 PACS number(s): 61.43.Bn, 61.72.Bb, 66.30.Dn, 71.15.Mb

I. INTRODUCTION

Pyrochlore-structured compositions have a wide range of technologically important properties, such as high ionic conductivity,[1] superconductivity,[2] luminescence,[3] and ferromagnetism.[4] Additionally, the Ti and Zr pyrochlores are candidates for the immobilization of actinides, particularly Pu from dismantled nuclear weapons.[5,6] The zirconate pyrochlores have been identified as being particularly resistant to radiation damage.[7–9] The pyrochlore structure, $A_2B_2O_7$, is a derivative of the fluorite structure, with two cations ordered on the A and B sites, and one-eighth of the anions missing. The anion vacancies are also ordered. Disordering of the cation sites coupled with oxygen disorder on the anion vacancies within the pyrochlore structure results in a defect-fluorite structure.[1,10] Many of the properties of pyrochlore, such as ionic conductivity, are very sensitive to the degree of disorder and related changes in the structure. Therefore, it is important to understand the energetics of the disordering process.

Chemical substitutions (e.g., Zr for Ti)[1] can induce the pyrochlore to defect-fluorite transition. For example, in the $Y_2(Ti,Zr)_2O_7$ system at room temperature, the introduction of 50% Zr appears to initiate disorder among the cation sites, associated with disorder among the oxygen sites with partial occupation of the vacancy.[1,11] With 90% Zr in the $Y_2(Ti,Zr)_2O_7$ system, the disorder between the cation sites and oxygen sites is complete, resulting in the defect-fluorite structure. In these samples at 1000 °C, the compositionally induced disorder allows for significant oxygen migration between the vacancies, leading to ionic conductivities up to 10^{-2} S/cm.[12,13]

In addition to compositionally induced disorder, irradiation of many pyrochlore compositions results in an order-disorder transition from the pyrochlore to a defect-fluorite structure, and finally, at higher doses, the aperiodic state.[14] $Y_2Ti_2O_7$ irradiated by 2 MeV Au^{2+} produces a buried defect-fluorite layer for low ion fluence (0.3 ions/nm^2) along with a completely amorphous layer.[15] The well-studied $Gd_2(Ti_y,Zr_{1-y})_2O_7$ compositional series shows a wide variety of behaviors from limited radiation tolerance for $y=1$ to complete tolerance (remaining as defect fluorite) for $y=0$.[7,9,16] A series of measurements has indicated the correlation between the critical amorphization temperature, above which no amorphization occurs regardless of radiation dose,[14] the enthalpy of formation from the oxides,[17] and the 3^+-cation (A-site) radius. These relationships point to the interdependence of the structural compatibility of the chemical species, the thermodynamic stability of the pyrochlore structure, and the recovery of ion beam-induced damage.

In an attempt to explain many of the experimental observations of order-disorder transitions in the pyrochlore system, as well as observed variations in radiation "tolerance" and ionic conductivity, many groups[18–23] have attempted to calculate the defect-formation energy of a large number of pyrochlore compositions. Contour maps of defect formation energies[19,20] as a function of A- and B-site cation radii show relatively constant values with respect to the A-site cation radius and relatively linear trends as a function of the B-site cation radius. This suggests the relatively greater importance

 ©2004 The American Physical Society

of the B-site over the A-site cation in determining the energetics of defect formation, a conclusion contradicted by irradiation experiments of rare-earth titanate pyrochlore compositions.[14]

These atomistic approaches rely on a classical pairwise model for interatomic bonding, which includes Coulomb interactions of point charges (the Madelung energy), van der Waals-like short-range attraction, and Born-Mayer type overlap repulsion.[18–20] Such calculations are computationally efficient and therefore allow for the calculation of large systems, as well as the testing of systems with a variety of atomic arrangements or compositions. Unfortunately, classical models do not treat atoms differently according to crystallographic position or coordination. Treating all oxygen atoms in the pyrochlore structure identically regardless of local environment, as is done in calculations using pair potentials, therefore neglects a possibly significant aspect of structural behavior and leaves the electronic structure of oxygen in an interstitial site undetermined. Moreover, Williford *et al.*[23] find that cation-antisite exchange energies in $Gd_2Ti_2O_7$ vary by more than an order of magnitude (0.12–3.53 eV) depending on the values of the parameters that are chosen for the pair potential model. This demonstrated sensitivity to the form of the pair potentials highlights the difficulty in using a classical approach when addressing defects requiring variable bond lengths and coordination.

The interpretation of experimental and classical modeling studies conflict on key issues related to the sequence of disordering and the relative importance of chemical species versus cation radius ratios. These may be due to physics that are not captured by the simple models including the local environment of each species, the nature of electronic bonding between atoms, and the length-scale over which the disorder occurs. First, atomistic modeling of a wide suite of compositions indicates physical and chemical properties in the pyrochlore system can be primarily explained by ionic radius alone. The implication of defect-formation energy contour maps resulting from classical methods is that the B-site cation radius can be used almost exclusively to explain defect formation energies, while a combination of the two cation radii control basic structural parameters such as the unit-cell volume and the location of placement of oxygen in the structure. This picture disagrees with ionic conductivity measurements on pyrochlore compositions with solid solutions on the B site, which do not show a smooth variation between end member compositions, indicating a more complex structural and chemical response to the mean size of the B-site cation.[1] Second, classical modeling approaches, which treat the oxygens on the normally occupied and normally unoccupied sites identically, find that the formation of oxygen defects must occur before disorder on the A- and B-cation site. Different experimental probes lead to apparently inconsistent conclusions regarding the primacy of cation or anion disorder: whereas diffraction studies indicate that oxygen disorder causes cation disorder, spectroscopic studies yield the opposite conclusion. Classical modeling studies do not resolve this apparent discrepancy because of their limitations: classical models that treat all the oxygen atoms equally, and all cation-oxygen bonds with the same model, may be biased towards oxygen disorder and smooth variations with compositional changes.

Therefore, it is imperative to "ground truth" atomistic models in quantum mechanical calculations that do not require assumptions about the form of the atomic interactions. In first principles methods based on density functional theory, energetics are derived directly from the solutions to the Kohn-Sham equations and are completely independent of experimental measurements: there are no free parameters in the theory. First-principles modeling can therefore examine the energetic behavior of the system with a high degree of disorder without constraints placed on the nature of bonding as in classical approaches. A basic understanding of the energetics of disorder in the yttrium pyrochlores, as they pertain to the ionic conductivity and its relationship to the structure, should therefore be directly applicable to the order-disorder transitions observed in other pyrochlore compositions.

We have calculated the structural properties of the ordered pyrochlore, as well as the energetics of cation-antisite defect formation, Frenkel-pair defect formation, and coupled cation-antisite and Frenkel-pair defect formation. Three pyrochlores, $Y_2Ti_2O_7$, $Y_2Sn_2O_7$, and $Y_2Zr_2O_7$, with B-site cation radii of 0.061, 0.069, and 0.072 nm, respectively,[24] provide a means by which to test the extent that changes in properties can be attributed to B-site cation radius, and whether some properties are more sensitive to the degree of covalent bonding. In addition, we have calculated the properties of the solid solution $Y_2(Ti_{0.25},Zr_{0.75})_2O_7$, with a mean tetravalent cation radius of 0.0691 nm, nearly identical to that of Sn^{4+}. This allows for the comparison of the relative importance of electronic configuration versus the mean ionic radius with respect to the behavior of the material. We explain deviations from simple trends with respect to cation radius by analyzing the computed valence band structure.

A. Pyrochlore structure

Pyrochlore is cubic ($Fd3m, Z=8, \mathbf{a}\cong 10$ Å), and the structural formula is ideally $^{VIII}A_2{}^{VI}B_2{}^{IV}X_6{}^{IV}Y$ (Roman numerals indicate the coordination number), where the A ($=Y^{3+}$) and B ($=Ti^{4+}, Sn^{4+}, Zr^{4+}$) are metal cations; X and Y are anions ($=O^{2-}$).[25] The pyrochlore structure is closely related to the fluorite-structure (AX_2), except there are two cation sites and one-eighth of the anions are absent (Fig. 1). The cations and oxygen vacancies are ordered. The loss of one-eighth of the anions reduces the coordination of the B-site cation from 8 to 6. The X-anion occupies the *48f* position; and the Y anion, the *8a* (when the origin of the unit cell is placed at the A site). All of the atoms in an ideal pyrochlore are on special positions, except the *48f* oxygen (O_{48f}). Thus, the structure is completely described by the cell edge, **a**, and the fractional coordinate (x) of O_{48f}. For the ideal structure the coordinations of the cations and anions are: $\mathbf{A}X_6Y_2, \mathbf{B}X_6, \mathbf{X}A_2B_2$, and $\mathbf{Y}A_4$. The unoccupied *8b* position, the site of the oxygen vacancy, is coordinated with four B-site cations, $[\,]B_4$. In the ideal pyrochlore structure, $x=7/16$ (0.4375), the B site is a regular octahedron and the A site is a distorted cube. For $x=3/8$ (0.375) the A-site polyhedron is a regular cube, and the B-site polyhedron is distorted to a trigonally flattened octahedron, with the topology of an oxygen-deficient ideal

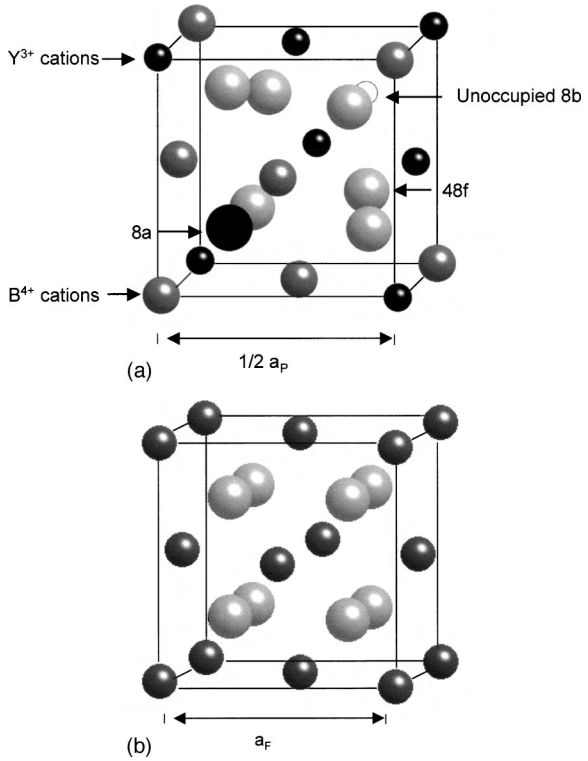

FIG. 1. The pyrochlore structure: The yttrium atoms are on the *16c* site (small black) and the 4+ cations are on the *16d* site (dark grey). The three different oxygen sites are the *8a* (large black), *48f* (light grey), and the vacant *8b* (open) sites. (a) Structure presented emphasizing the oxygen arrangements and similarity to the fluorite structure, (b), where complete disorder within the cation sites and oxygen sites results in the fluorite structure.

fluorite structure. Compositions with the pyrochlore structure can take on x values anywhere between these two ideal values, with polyhedral shapes smoothly varying between the shapes as described for the ideal pyrochlore and fluorite structures. The result is a relatively simply described structure with a great degree of structural flexibility.

B. Disordered pyrochlore structures

In addition to fully ordered, and fully disordered (defect fluorite) states, partial disorder is commonly observed. The partially ordered state is challenging to characterize experimentally, but important because it may reveal the underlying causes of disorder. One must consider the degree of order on cation and anion sublattices and the length scale of disorder. Different experimental probes of the partially disordered state may lead to apparently different conclusions because they are sensitive to different length scales, or are more sensitive to either the cation or anion sublattice disorder.

Diffraction studies are sensitive to long-range disorder, i.e., on length scales of thousands of unit cells. X-ray diffraction will be more sensitive to disorder on the cation than on the anion sublattice. Reitveld refinement of neutron and x-ray diffraction patterns detect the onset of oxygen disorder in the $Y_2(Ti_{1-y},Zr_y)_2O_7$ system at $y=0.3$. The onset of compositionally-induced disorder on the cation lattice occurs at $y<0.5$, with significant increase in the occupation of the *8b* oxygen site associated with onset of disorder on the cation sites.[26] Complete disorder on the cation and oxygen lattices occurs at $y=0.9$, with the material taking on a defect-fluorite structure [Fig. 1(b)].

The ionic conductivity is sensitive to local structure, via the migration energy of oxygen. Therefore, the oxygen defect formation energy, as a proxy for migration energy, is important for understanding conductivity measurements.[1,26] Experimental data on ionic conductivity cannot disentangle the effects of disorder and composition in the $Y_2(Ti_{1-y},Zr_y)_2O_7$ system. The ionic conductivity in this system increases with increasing Zr content up to 60 at. % Zr, but does not increase significantly with further incorporation of Zr, despite increasing disorder.

Vibrational spectroscopy is sensitive to the degree of local order.[11,27,28] In the pyrochlore structure, infrared and Raman spectroscopy are primarily sensitive to oxygen-cation vibrations,[29] and lack sensitivity to the cation antisite disorder or oxygen vacancy population. Vibrational spectroscopy indicates that irradiation-driven disorder in the $Gd_2(Ti,Zr)_2O_7$ system is driven by cation disorder.[11]

Thermochemical measurements in the $Gd_2(Ti,Zr)_2O_7$ system indicate that the enthalpies of formation of the fully ordered structure and the defect-fluorite structure are nearly indistinguishable[30] (<10 kJ/mol). This would indicate that the energy of long-range ordering is insignificant compared to the energies of local cation and oxygen vacancy ordering. Therefore, local cation- and oxygen-defect-formation energies calculated on short length scales (<1 unit cell) should help to elucidate the differences in experimental conclusions.

II. METHODS

The basis for these calculations is density functional theory (local density approximation), with Vanderbilt-type ultrasoft pseudopotentials.[31,32] All calculations are performed with the Vienna *ab initio* simulation package (VASP).[31,33–35] Results are static (0 K) and ionic positions are relaxed according to the calculated forces on each atom. Computations are based on the primitive unit cell (two formula units: 22 atoms), a $2\times2\times2$ Monkhurst-Pack k-point mesh, and a cutoff energy of 600 eV, except where otherwise stated. Tests show these computational parameters are sufficient to converge the total energy to within 1 meV and the equilibrium volume to within 0.02%.

The differences in the calculated total energy between the ordered and disordered state indicate the relative stability of those states, as well as the energy required to induce disorder in the material. Comparing the energetics of single defects with coupled cation-oxygen defects gives a measure of the relative importance of cation and oxygen defects.

In contrast to the Mott-Littleton models[19] that study defects in finite nanocrystals embedded in a polarizable medium, our systems are infinite and periodic, so that defects are periodically repeated. In our calculations, defects are separated by no more than 0.74 nm, which is 25% smaller than the nanocrystal used in previous Mott-Littleton calculations.[20] Even so, we find that our calculations are in

the dilute limit for single defects: the lattice distortion caused by the defect decreases rapidly with increasing distance from the defect and reaches essentially zero within the translational repeat unit.

In order to compare more directly with room-temperature experimental observations, we have estimated the effects of lattice vibrations based on a simple model of the vibrational density of states.[36] We consider the pressure due to zero-point motion, P_{zp}:

$$P_{zp} = \frac{9n\gamma}{8}\frac{k_B\Theta_D}{V}, \tag{1}$$

where Θ_D is the Debye temperature, k_B is Boltzmann's constant, γ is the Grüneisen parameter, and V/n is the mean volume per atom. Assuming $V/n = 11.4$ Å^3 and nominal values for Θ_D and γ (1000 K and 1, respectively) the P_{zp} correction is 1.4 GPa.

The effect of 300 K thermal energy, E_{th}:

$$E_{th} = 9nk_BT(T/\Theta_D)\int_0^{\Theta_D/T} x^2 \ln\left(1 - e^{-x}\right)dx \tag{2}$$

can be expressed as a thermal pressure

$$P_{th} = -\left(\frac{\partial E_{th}}{\partial V}\right)_T = \frac{\gamma}{V}E_{th}, \tag{3}$$

where T is the absolute temperature. This adds an additional factor of 0.3 GPa, for a total pressure correction of 1.7 GPa.

A. Pyrochlore structures

As a starting point for energetic comparisons, we performed full structural relaxations of the ordered pyrochlore structures: $Y_2Ti_2O_7$, $Y_2Zr_2O_7$, $Y_2(Ti_{0.25},Zr_{0.75})_2O_7$, and $Y_2Sn_2O_7$. Of these compositions, $Y_2Zr_2O_7$ is unstable in the pyrochlore structure and is included in our suite of systems in order to illustrate energetic trends. Calculations of $Y_2(Ti_{0.25},Zr_{0.75})_2O_7$ were performed by substituting one of every four Zr atoms in the primitive unit cell with a Ti atom, while maintaining the systematic oxygen vacancy in the *8b* site. This composition is found to form the pyrochlore structure, but with a significant degree of both cation and anion disorder.[1] This solid solution also has approximately the same mean B-site cation radius as Sn^{4+} (0.069 nm), allowing for the comparison of different compositions with similar ionic radii.

B. Defect formation energies

Defect formation energies were calculated by moving cations, oxygen atoms, or both, within the structure and by relaxing the entire structure to minimize the forces on the atoms. The defect formation energy is then calculated as the difference between the total energy of the stable structure and the relaxed defect structure at constant volume.

Single and double cation exchange models were performed as cation antisite reactions[37]

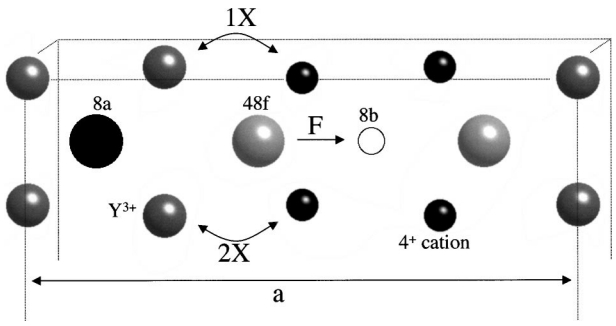

FIG. 2. The pyrochlore structure: Atom symbols are as in Fig. 1. In models of disorder, neighboring *16c*- and *16d*-site cations are swapped. For 1X models, one cation-antisite pair is created, and for 2X models, two neighboring cation-antisite pairs are created. In the case of the "2X" models, the cation arrangement around the *48f*, *8a*, and *8b* sites are identical. Frenkel defects are formed by moving the *48f* oxygen enclosed by the cation-antisite defects to the *8b* site, labeled F.

$$A_A + B_B \rightarrow A_B' + B_A^{\bullet}. \tag{4}$$

Exchanges are performed as in Fig. 2, where 1X represents a single exchange and 2X indicates a second such exchange from the cation-ordered (0X) state. For the 2X case, the exchange is chosen such that the cation environment surrounding a single *48f* oxygen is identical to the neighboring *8a* and *8b* sites, i.e., 48*f*, *8a*, and *8b* sites are each surrounded by two A and two B cations in the (100) plane as shown in Fig. 2. This is a "compact" arrangement of the defects[23] in contrast to an "open" arrangement in which the two defects are at greater distance from each other. Despite the relatively small size of the primitive unit cell, we have found that the compact two-defect calculation (2X) is essentially in the dilute limit: calculations show identical (0.9% difference) 2X defect formation energies when defect pairs are separated by ~0.25 nm (primitive cell) or ~1 nm (conventional cell).

Frenkel defect formation energies were calculated by the difference between the stable structure (either cation-ordered or with one or two cation-antisite defects) and the energy of the unrelaxed structure with a Frenkel defect according to the reaction

$$O_{48f} \rightarrow V_{48f}^{\bullet\bullet} + O_{8b}'' \tag{5}$$

such that any oxygen migration is assumed to occur through a *48f*–*8b*–*48f* path.[22] We considered two alternative oxygen migration paths. The *8a*–*8b* path is expected to be highly unfavorable because of an intervening tetravalent cation.[37] We confirmed this expectation with calculations of the unrelaxed structure with the Frenkel defect

$$O_{8a} \rightarrow V_{8a}^{\bullet\bullet} + O_{8b}''. \tag{6}$$

While direct *48f*–*48f* hopping is not hindered by intervening atoms, the hopping distance is 25% greater than one with an intermediate state of *8b* and such calculations would require including noncharge balanced vacancies.[18]

In this work, the reported Frenkel-pair formation energies are based on the unrelaxed structures, as they are found to be unstable in the absence of cation antisite defects (0X). Re-

TABLE I. Fully ordered structural parameters for yttrium pyrochlore.

	R_B (nm)[a]	a_0 (nm)	x-O_{48f}	K_0 (GPa)[b]
$Y_2Ti_2O_7$ VASP	0.0605	1.0049	0.4204	205.2(±3.6)
		1.0084 (300 K)		
$Y_2Ti_2O_7$ Farmer		1.01002(6)	0.4200(4)	
$Y_2Sn_2O_7$ VASP	0.069	1.0329	0.4120	190.7(±0.8)
		1.0363 (300 K)		
$Y_2Sn_2O_7$[g]		1.03723	0.4118(9)	
$Y_2(Ti_{0.25}Zr_{0.75})_2O_7$ VASP	0.0691	1.0360	0.4105	192.9(±4.6)
$Y_2(Ti_{0.25}Zr_{0.75})_2O_7$[h]		1.0332	0.3900(3)[d]	
$Y_2Zr_2O_7$ VASP	0.072	1.0463	0.408	176.2(±2.6)
		1.0496 (300 K)		
$Y_2Zr_2O_7$[c]		1.0411[e]	0.41[f]	

[a]Sixfold coordination.
[b]$K' = (dK_0/dP)$ is assumed to be 4.
[c]Significant amount of cation and oxygen disorder.
[d]Approximate uncertainty.
[e]Extrapolated from Heremans *et al.*[26]
[f]Systematics from Pirzada *et al.*[18]
[g]See Ref. 44.
[h]See Ref. 26.

laxing the structure always results in the oxygen returning to its initial position. Therefore, Frenkel-pair formation energies may be overestimates. Further, all defect calculations were performed at constant volume: defect formation may alter the volume at constant pressure, an effect that we have ignored. However, we have found that the energy differences are small: no more than 0.05 eV/defect.

The coupled cation-antisite/Frenkel-pair defect formation energy was calculated from the fully relaxed structure containing a cation-antisite and a Frenkel defect [i.e., combining reactions (4) and (5)], which was found to be mechanically stable. We consider the compact defect arrangement here for coupled cation-antisite and Frenkel-pair defect formation energy calculations. In each case, the *48f* oxygen that was used in the Frenkel defect reaction was the one enclosed by the cation-antisite defect (first nearest neighbor instead of second), and it was in all cases that oxygen that experienced the greatest distortion from its stable site in the direction of the *8b* site in reaction (4). Williford *et al.*[23] showed that the geometry of the cation-antisite defects affects the oxygen migration energy, such that compact defects, where nearest neighbors are involved in the defect formation, have the lowest defect formation energies and lowest associated oxygen migration energies. In contrast, an open cation disorder model involves defects with second nearest cation neighbors (~0.45 nm instead of 0.2–0.25 nm for first nearest neighbors). Williford *et al.*[23] showed that for all pair potential models examined, there are no open cation disorder models that are stable with respect to Frenkel defect formation.

C. Electronic structure

The charge on each ion in the relaxed structure is estimated by integrating the valence charge density within the Wigner-Seitz spheres about each atom. The Wigner-Seitz radius for each atom is chosen such that the total volume in the summation was approximately 100% and that the ratios of the atomic radii were equal to that of the actual ionic radii.[24] The band structures of the ordered structures are calculated along high symmetry lines in the Brillouin zone. The *spd*-partial density of states is determined for each atom from the projection of the angular momentum of the charge onto the same Wigner-Seitz spheres as used in the ionic charge determinations. The partial density of states is calculated with a $12\times12\times12$ *k*-point grid smoothed and the tetrahedron method.[34]

III. RESULTS

A. Ordered structures

The fully ordered zero-pressure, static lattice parameters, oxygen positional parameter, and bulk modulus for each composition are shown in Table I and Fig. 3. VASP accurately reproduces the experimentally determined lattice parameters for $Y_2Ti_2O_7$ and $Y_2Sn_2O_7$ to within 0.8% and 0.6%, respectively, when the effects of thermal pressure are considered. For $Y_2Ti_2O_7$ and $Y_2Sn_2O_7$, x-O_{48f} is found to be within experimental error of the reported experimental value. The zero-pressure lattice parameter (1.0463 nm) and the oxygen position (0.408) for the $Y_2Zr_2O_7$ pyrochlore is consistent with systematics of R_A/R_B in the fully ordered pyrochlore system.[20] For the $Y_2(Ti_{0.25}Zr_{0.75})_2O_7$ solid solution, the 300 K corrected-lattice parameter agrees with experimental measurements to within 1.5%,[26] but we predict a much greater mean x-O_{48f} than measured. This reflects the fact that these calculations have no A-B site cation mixing and completely ordered oxygen vacancies; whereas, for the experimental

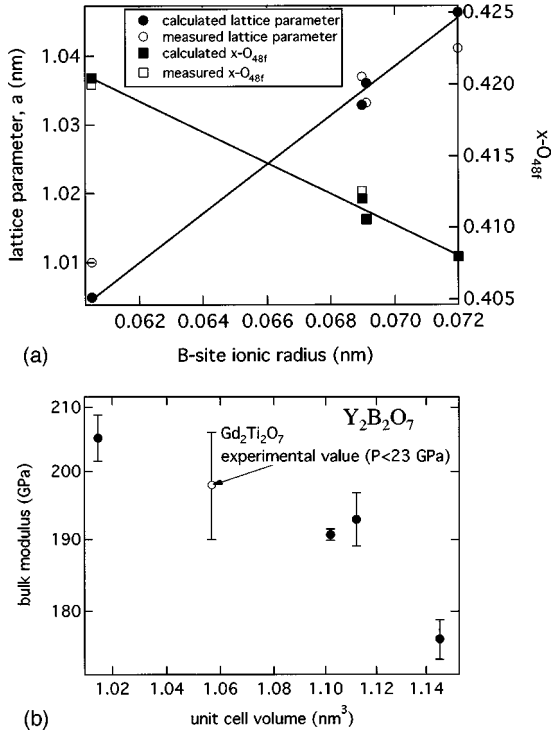

FIG. 3. Static structural parameters as a function of B-site cation radius: (a) lattice parameter, circles, and the *48f* oxgyen's *x* parameter, squares. Open circles represent room temperature, experimentally determined values. The lattice parameter for $Y_2Zr_2O_7$ is an extrapolation of lattice parameter systematics in the $Y_2(Ti_x,Zr_{1-x})_2O_7$ system.[26] The experimentally derived *x* parameter for the solid solution is not shown (0.390),[26] and reflects significant disorder in the structure. (b) Bulk modulus assuming the pressure derivative of bulk modulus $dK_0/dP=4$.

measurements there is significant disorder on both the cation and anion lattices.[1]

Variation in unit-cell volume as a function of pressure allows the determination of the bulk modulus, a measure of the strength of interatomic bonds. Comparisons between calculations and experimentally derived bulk moduli are an additional test of our theoretical methods, as it is a higher order derivative of the total energy. The bulk modulus of $Gd_2Ti_2O_7$, based on quasihydrostatic compression to 24 GPa, is 198(±8) GPa, in general agreement with our results and expectations based on cation radius systematics [Fig. 3(b)].[38] Our predicted bulk moduli and the bulk modulus of $Gd_2Ti_2O_7$ are substantially lower than those estimated for zirconate pyrochlores from a semiempirical relationship between elastic energy and ionic conductivity.[38]

Examination of the electronic band structure shows that the ⟨Sn-O⟩ bond is substantially more covalent than the ⟨Ti-O⟩ or ⟨Zr-O⟩ bond. The oxygen 2*p* band width in the stannate is 7.6 eV, as compared with 4.3 eV and 4.1 eV in the titanate and zirconate, respectively [Fig. 4(a)]. Moreover, the partial density of states show substantially more hybridization of the O_{48f} 2*p* states with the Sn 4*d* states than of the O_{48f} 2*p* with the Ti 3*d* states [Fig. 4(b)]. These results support expectations based on electronegativity differences, which lead to the classification of the ⟨Sn-O⟩ bond as polar covalent, and the ⟨Ti-O⟩ and ⟨Zr-O⟩ bonds as ionic.

The total electronic charge on the oxygen atoms varies significantly between the *48f* oxygen and oxygen placed on the *8a* or *8b* sites, with differences of up to 10%, generally consistent with the first-principles Hartree-Fock study[21] of $La_2Zr_2O_7$. However, with the introduction of a single neighboring cation defect, the magnitude of the difference between the two oxygen positions decreases to no more than 5%, reflecting the greater similarity in environment about each oxygen site with respect to cation coordination. The greatest difference is between the O_{48f} and V_{8b} sites in $Y_2Ti_2O_7$, the composition with the greatest *x*-O_{48f} positional parameter [Fig. 3(a)] and generally largest defect formation energies. Indeed, the partial density of states for the oxygen 2*p* electrons show significant differences between the *8a* and *48f* sites, with the greatest differences in the $Y_2Ti_2O_7$ pyrochlore composition [Fig. 4(b)].

B. Oxygen defect formation energy for perfectly ordered cations (0X)

In the cation-ordered structure, oxygen is not stable in the *8b* site. The Frenkel-pair formation energies are large (several electron-volts) in all compositions (Table II). The Frenkel-pair formation energy for reactions (5) and (6) in $Y_2Zr_2O_7$ is 3.3 and 3.7 eV less, respectively, than $Y_2Ti_2O_7$ as expected from the greater ionic conductivity of the zirconate. However, the calculated Frenkel-pair formation energies for $Y_2Sn_2O_7$ are 2.9 and 3.3 eV greater than $Y_2Zr_2O_7$, and are within 6% of the value for $Y_2Ti_2O_7$. The similarity between the calculated oxygen defect values for $Y_2Sn_2O_7$ and $Y_2Ti_2O_7$ is found despite the very different R_A/R_B ratios and different values for *x*-O_{48f}, lattice constant and bulk modulus in the ordered structure [Fig. 5(a)].

The $Y_2(Ti_{0.25}Zr_{0.75})_2O_7$ solid solution has two possible defect formation energies depending on whether the oxygen involved in the defect was originally neighboring a titanium atom or not. In the case of a *48f* oxygen without a titanium nearest neighbor, the Frenkel-pair formation energy is within 0.4 eV of the value for the $Y_2Zr_2O_7$ end member value of 4.2 eV. When the *48f* oxygen is initially adjacent to one titanium atom and one zirconium atom (Fig. 2), the Frenkel-pair defect formation energy is almost exactly the average of the Ti and Zr end member values of 7.5 and 4.2 eV, respectively, with a Frenkel-pair formation energy of 6.4 eV (Table II). A weighted average of these defect energies [Fig. 5(a)] indicate that the solid solution varies linearly with the cation radius ratio R_A/R_B in the Ti-Zr solid solution series.

For purposes of comparison to previously published calculations,[22] we also approximated the Frenkel defect formation energy through a thermodynamic cycle. Wilde and Catlow[22] estimated the Frenkel-pair defect formation energy from the reaction (Table III):

$$[A_4B_4O_{13}]^{2+} + [A_4B_4O_{15}]^{2-} = 4A_2B_2O_7, \qquad (7)$$

where the positively charged structure lacks either a *48f* or *8b* oxygen, and the negatively charged structure has an extra oxygen on the normally vacant *8a* site. Our first principles results for reaction (7) are within 20% of those for reaction

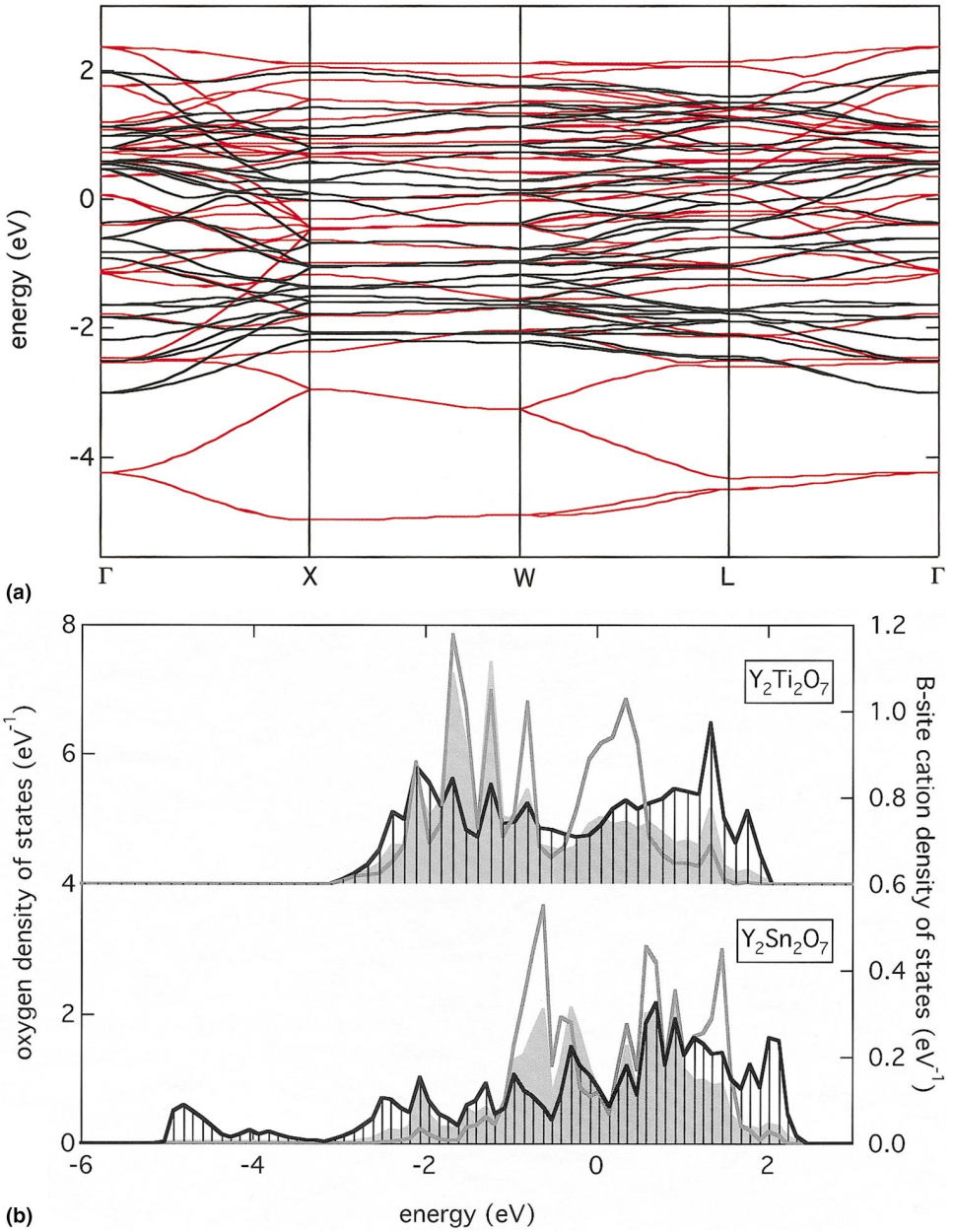

FIG. 4. (Color) (a) Valence (O 2*p*) bands for ordered $Y_2Sn_2O_7$ (red) and $Y_2Ti_2O_7$ (black). (b) Partial density of states of oxygen 2*p* electrons (O_{48f} black with bars; *8a*O*8a* grey curve) showing overlap with the Ti (grey fill; top) and Sn (grey fill; bottom) *p* electrons.

(5). Although reaction (7) allows for full structural relaxation while reaction (5) does not, we prefer the energy of reaction (5) as the best estimate of the Frenkel defect formation energy because reaction (7) entails additional repulsion of oxygen atoms in $[A_4B_4O_{15}]^{2-}$ and of cations in $[A_4B_4O_{13}]^{2+}$. Our calculations of the energy of reaction (7), as for our other calculations, were performed at constant volume; we found that the difference in pressure between the positively and negatively charged structures is 4.4 GPa for the Ti end member that would amount to only 0.1 eV in the reaction energy. Our first principles values for reaction (7) are within a factor of 2 of those from the atomistic model, and there is partial agreement between first principles and atomistic approaches in the relative magnitude of the reaction energies (Table III).

C. Cation-antisite formation energies

Because of the greater similarity in cation size, an exchange between Y^{3+} and Zr^{4+} should be more compatible in the structure than with Sn^{4+} or Ti^{4+}. Indeed, the cation defect formation energies for both 1X and 2X exchanges (Fig. 2) are lower in $Y_2Zr_2O_7$ than the other two end member compositions (Table II). $Y_2Ti_2O_7$ and $Y_2Sn_2O_7$ show almost identical defect formation energies, despite the large difference in B cation radius. [Fig. 5(b)]. The two different possible 1X cation-antisite defects in the solid solution, Ti^{4+}-Y^{3+} exchange and Zr^{4+}-Y^{3+} exchange, have energies nearly identical to those of the corresponding end member, indicating the very local effects of the cation-antisite defect [Fig. 5(b)]. 1X cation-antisite defect formation energies are

TABLE II. Defect formation energies.

		Cation antisite formation (eV)		Frenkel-pair formation energy (eV)			
	R_B/R_A[a]	1X	2X	0X (*48f–8b*)	0X (*8a–8b*)	1X	2X
$Y_2Ti_2O_7$	0.594	1.77	8.405	7.514	10.805	3.783	1.906
$Y_2Sn_2O_7$	0.677	1.97	7.037	7.0483	10.4125	3.326	3.571
$Y_2(Ti_{0.25}Zr_{0.75})_2O_7$	0.678				8.228		
Ti–Y		1.75	3.41	6.403		1.129	···
Zr–Y		0.03	3.40	4.586	0.377	1.989	1.175
$Y_2Zr_2O_7$	0.707	0.258	3.046	4.192	7.146	0.896	0.637
			3.074[b]				

[a]Cation ratios are for sixfold coordination for the B-site cation and eightfold coordination for the A-site cation.
[b]88-atom unit cell.

about 25% of the Frenkel-pair formation energies in the ordered cation lattice. The 2X exchange energy is 3.5–11 times larger than the 1X exchange energy (Table II) for a given composition, where the solid solution shows similar effects as the 1X case, where the energetics of the second exchange, which must be Zr^{4+}-Y^{3+} in the primitive lattice resembles the exchange energies of $Y_2Zr_2O_7$.

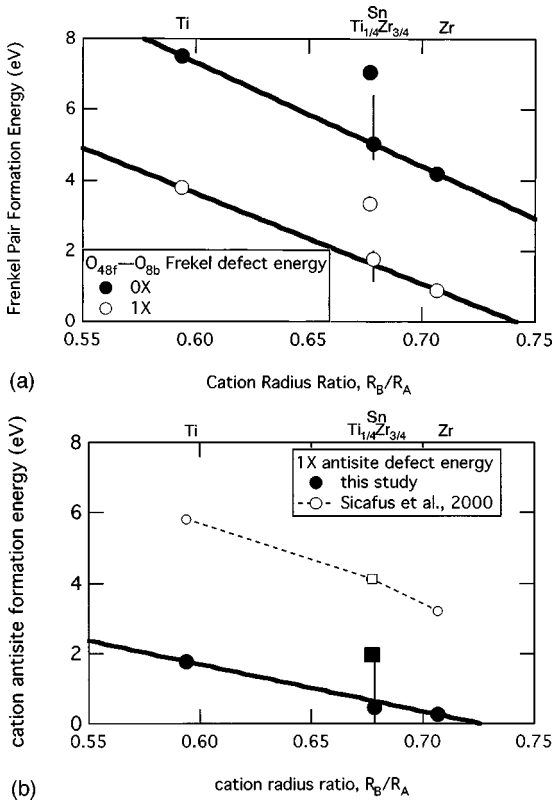

FIG. 5. Defect formation energies as a function of cation radius ratio R_A/R_B. (a) Frenkel defect energies for 0X (solid) and 1X (open) cation antisite defects and (b) 1X antisite defect energies (solid) compared to defect energies as derived from an atomistic model[19] (open). The defect energies for the $Y_2(Ti_{0.25}, Zr_{0.75})_2O_7$ are plotted as a weighted average according to the Zr/Ti ratio, with the vertical bar indicating the range of the individual defect energies (Table II). In each case the Sn-end member (squares) plots significantly above the trend for the Ti-Zr solid solution series.

D. Coupled cation-antisite and Frenkel-pair formation energies

Frenkel-pair formation energies associated with cation defects are about half (3.8 eV for $Y_2Ti_2O_7$) the calculated value in the cation-ordered lattice (7.5 eV for $Y_2Ti_2O_7$). Therefore, the presence of cation-antisite defects lowers the oxygen defect formation energy, thereby facilitating oxygen migration through the lattice. In all cases the Zr end member case has coupled cation-antisite and Frenkel-pair defect formation energies that are more than 2 eV lower than the Sn or Ti cases, reflecting the greater similarity in oxygen and cation sites. The low (<1 eV) coupled cation-antisite and oxygen Frenkel-pair formation energy explains why $Y_2Zr_2O_7$ does not form the ordered pyrochlore structure, but rather the defect-fluorite structure, due to the scant energetic advantage of cation and oxygen vacancy ordering.

The calculated values for Frenkel-pair defect formation energies in the presence of cation-antisite defects in the $Y_2(Ti_{0.25}Zr_{0.75})_2O_7$ solid solution show values intermediate between the end members, as was found for the 0X calculation [Fig. 5(a)]. The Frenkel-pair formation energies reflect the very local cation environment such that the individual defect energies are similar to the end member values. However, for the 1X and 2X Frenkel-pair defects, the energies are not as easily correlated to the end members because of the greater degree of disorder. In the case of annealed solid solutions, these results imply more Zr^{4+}-Y^{3+} defects than Ti^{4+}-Y^{3+} defects due to their lower energies. Based on the relative energetics of Zr^{4+}-Y^{3+} defects ($\sim$0 eV) as compared with Ti^{4+}-Y^{3+} defects ($\sim$1.75 eV) (Table II), in sample synthesis, annealing of the Ti^{4+}-Y^{3+} defects has a greater energy benefit. Further, these cation-antisite defects should tend to associate with oxygen Frenkel-pair defects. As the solid solution becomes richer in titanium, the annealing process can more easily result in an ordered structure, as reflected by the varying amounts of disorder across the titanium-zirconium solid solution series. This picture should be testable by a combination of x-ray and neutron diffraction.

As seen in the 0X Frenkel pair formation and 1X and 2X cation-antisite reactions, the 1X Frenkel pair formation energy is almost identical for $Y_2Ti_2O_7$ and $Y_2Sn_2O_7$ (3.8 and 3.3 eV), but is more than 2.8 eV greater than $Y_2Zr_2O_7$ (Table

TABLE III. 0X Frenkel-pair formation energies computed via thermodynamic cycle.

	Wilde and Catlow[22]		VASP		Ratio[a]	
	$Y_2Ti_2O_7$	$Y_2Zr_2O_7$	$Y_2Ti_2O_7$	$Y_2Zr_2O_7$	$Y_2Ti_2O_7$	$Y_2Zr_2O_7$
48f–8b	4.60	3.27	8.63	5.00	0.871	0.838
8a–8b	7.96	9.82	9.82	6.21	0.909	0.870

[a]Ratio of 0X Frenkel pair formation energy computed by VASP using our charge-balance method (Table II) to that using the thermodynamic cycle.

II). Moreover, the behavior of Sn^{4+} is dramatically different from Ti^{4+} and Zr^{4+} in the solid solution, with the 0X Frenkel-pair formation energies for the solid solution being 10%–35% lower than the Sn end member value of 7.05 eV. Therefore, any attempt to predict the behavior of $Y_2Sn_2O_7$ based on the average cation radius, x-O_{48f}, or lattice constant would greatly underestimate the Frenkel pair formation energies.

IV. DISCUSSION

A. R_A/R_B constraints on pyrochlore stability

The calculated structural parameters (lattice parameter, x-O_{48f} and bulk modulus) are linearly dependent upon the B-site cation radius, with the mean B-site cation radius for the solid solution apparently representative for the purposes of lattice size and oxygen position [Fig. 3(a)]. Indeed, the bulk modulus is also linearly dependent upon the unit-cell volume [Fig. 3(b)], indicative of the influence of the B-site cation radius on the strength of the ⟨B-O⟩ bond and consistent with results in compositional variations in other structures.[39] When compared to $Y_2Sn_2O_7$, the $Y_2(Ti_{0.25}Zr_{0.75})_2O_7$ has an almost identical lattice parameter, mean oxygen position and bulk modulus.

Based on the similarities of the lattice constant, mean x-O_{48f} and compressibility of two compositions with the same mean B-site cation radius, it appears reasonable to assume that compositions in a solid solution can be synthesized to attain desired physical properties intermediate between those of end member compositions with the pyrochlore structure. One can imagine "tuning" pyrochlore properties by compositional changes in the appropriate binary systems. As an example, because x-O_{48f} is correlated to radiation tolerance[14] and compressibility (through unit-cell volume), a pyrochlore solid solution could be synthesized to produce desired properties under radiation with a particular compressibility by choosing cations based on their ionic radii. Decreasing unit-cell volume with decreasing B-site cation size increases x-O_{48f}, moving the structure closer to ideal pyrochlore and in general accord with previous modeling results.[40] This general result is supported by atomistic modeling of a broad range of compositions, showing approximately equal dependence on the A- and B-site cation radii[40] with x-O_{48f} changing as a function of unit-cell volume at a rate of $-9.2\times10^{-5}/\text{Å}^3$. Changing R_A and R_B while leaving the R_A/R_B radius ratio constant leaves the O_{48f} position largely unchanged, by simply expanding or contracting the structure. This is in contrast to the effect of decreasing unit-cell volume through increasing pressure. The effect of pressure appears to shift x-O_{48f} closer to the ideal fluorite, but with a shallow slope of $1.5\times10^{-5}/\text{Å}^3$, just 15% of the magnitude of slope due to compositional changes. Therefore, x-O_{48f} is dependent upon the radius ratio R_A/R_B and the compression of the structure due to pressure.[41]

In contrast to average structural properties, defect energetics are not simple functions of ionic radius, or radius ratios, but instead are much more sensitive to other aspects of the electronic structure. The relative importance of covalent and ionic bonding, and the importance of *d* electrons in the ⟨Sn-O⟩ bond are not easily captured in spherically symmetric atomistic models. For example, the nearly identical defect formation energies in the Ti and Sn end members were not evident in previous atomistic modeling studies[18,19] which show a much more linear trend as a function of B-site cation radius. Increased charge sharing between Sn^{4+} and O^{2-} ion relative to the more ionic ⟨Ti-O⟩ and ⟨Zr-O⟩ bonds increases the defect-formation energy relative to that expected based on an assumed linear relationship with cation radius in the B-site (or, more generally, the R_A/R_B ratio; Fig. 5). These are not purely ionic systems, and the effect of electronic structure on bonding is important.

The defect formation energies in a crystal are generally related to the radiation tolerance of the material.[19] Naguib and Kelly[42] correlated the radiation tolerance of nonmetallic solids with the relative ionicity of the material, finding more covalently bonded materials sustain greater amounts of damage (that is they are more readily amorphized) at lower temperatures under heavy ion irradiation. The defect formation energies presented here are not consistent with the general criteria of Naguib and Kelly.[42] $Y_2Sn_2O_7$ is one of the most radiation resistant of the pyrochlores,[43] but it shows no evidence of amorphization at fluences of more than 6×10^{15} ions/cm^2 at room temperature, even though it is significantly more covalent in its bonding than $Y_2Ti_2O_7$ or $Y_2Zr_2O_7$. We note, however, that the 72 compounds used in the study by Naguib and Kelly were all diatomic materials forming generally simple structures without the structural complexity and flexibility of pyrochlore.

B. Order to disorder transitions in pyrochlore

A key question in understanding the pyrochlore to defect-fluorite transition is how defects on the oxygen and cation lattice proceed to result in the disordered structure. In the calculations presented here, oxygen defects were not found

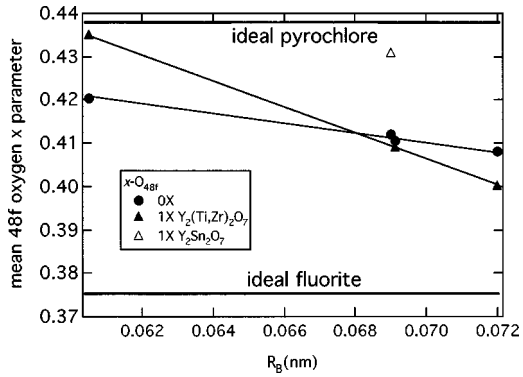

FIG. 6. The effect of cation defects on the mean *x* parameter of the oxygen in the *48f* oxygen site as a function of B-site cation radius. Circles, no cation defect; and triangles for 1X.

to be stable upon relaxation without the presence of associated cation defects. This, together with the fact that the Frenkel-pair formation energies are large for all compositions, indicates that oxygen defect formation independent of cation defects is unlikely. Together with our finding that the Frenkel-pair formation energy is substantially lowered in the presence of a cation antisite defect, our results indicate that cation disorder *causes* local oxygen disorder.

The primacy of cation defects can be understood in terms of changes to the structure of the oxygen sublattice in response to the antisite defect. In the case of cation antisite defect formation with initially ordered oxygen vacancies, the relaxed structure results in a *48f* oxygen atom located closer to the *8b* site than the original *48f* site. The mean x-O_{48f} parameter is often taken as a predictor of radiation tolerance, with those compositions with O_{48f} positions closer to the ideal fluorite arrangement ($x=0.375$) being most "resistant" to amorphization.[14] In the $Y_2Zr_2O_7$ 1X case, one originally O_{48f} relaxes 0.132 nm away from its 48*f* position so that it is only 0.0868 nm from the *8b* site, or 60% of the distance between the *48f* and the normally vacant *8b* site. That is, the 1X cation-antisite defect causes relaxation of an oxygen atom to a position closer to the vacancy than to its original *48f* site. This allows for a short hopping distance as compared with the anion-ordered structure with 0.219 nm between *48f* and *8b* sites. The mean oxygen positional parameter decreases from 0.408 to 0.400, or 24% closer to the ideal fluorite position (Fig. 6). A shift of this magnitude is at the limits of resolution of x-ray diffraction analysis (see uncertainties in Table I), yet is shown by our calculations to be energetically significant. Similarly, for the case of $Y_2Ti_2O_7$, the mean x-O_{48f} decreases to 0.406 from 0.420 (31% closer to ideal fluorite), but the minimum *48f*–*8b* distance, 0.114 nm, is only shifted 45% of the way from the *48f* to *8b* site, compared to 60% in the Zr end member case. Using the mean x-O_{48f} in the 1X and 2X cases as a proxy for a system with an equivalent population of defects, but with random orientations, the B-site contains 25% A cations and vice-versa, but with only 8.3% (1 of 12) oxygen occupancy of the *8b* site. Therefore, some extreme local distortion to the oxygen arrangement may be averaged out in diffraction measurements, masking the local effects of cation disorder.

The interpretation of the order-disorder process based on defect-formation energies is different than the interpretation of transmission electron microscopy diffraction results for Lian *et al.*[10] Ion-beam irradiated samples appear to show greater Frenkel-pair defects than cation-antisite defects, implying that oxygen defects precede the formation of cation defects. This can be reconciled with the theoretical results presented here by considering the differences in the process by which disorder is induced. In the case of the study here, defects are introduced without regard to any recovery process. In ion-beam experiments, the region disturbed by the heavy ion bombardment must recover from the high-energy state in the bombardment process to a pyrochlore-like structure over extremely short time scales (~ps). Therefore, the system cannot be considered annealed and, only local ordering can be attained. Therefore, in the ion-beam recovery process, the energetics of longer-range ordering is insignificant. The relative energy gain in local ordering of cations is greater than the energy gain involved in ordering the oxygen atoms. Therefore, the cation lattice is established much more readily than the oxygen lattice during ion-beam irradiation as an effect of the energetic advantage to ordering the cations instead of a cation-ordered structure with a significant population of oxygen defects being stable. The results here are more applicable to the interpretation of the vibrational spectroscopy results (e.g., Ref. 11) in which cation site disorder appears to lead oxygen disorder. Thermochemical measurements of the $Gd_2(Ti,Zr)_2O_7$ system further support the interpretation here, showing that the energetics of long-range ordering is minor in comparison to local disorder.[30]

V. CONCLUSIONS

In contrast to the lattice parameter, x-O_{48f} and bulk modulus systematics in the ordered pyrochlore structures, the cation defect formation energies do not depend simply on cation radius, but are sensitive to other aspects of the electronic structure. The more covalently bonded stanate is much more resistant to defect formation than trends based on cation radius for more ionic compositions would indicate. In this study, we have demonstrated the complementary effects of atomic size and electronic configuration, that is the bond type, on the energetics of the disordering process.

Our results indicate that cation antisite disorder precedes oxygen disorder. Cation antisite formation energies are much lower than Frenkel-pair formation energies. Moreover, the energetics of Frenkel-pair formation become much more favorable in the presence of a cation antisite defect. Our inference is consistent with that drawn from vibrational spectroscopic studies and thermochemical data.

Conclusions based on trends in data in the ordered pyrochlore system cannot be directly used to predict the properties of a disordered pyrochlore. Likewise, synthesizing a solid solution to attain a desired property intermediate to those of the end members may not result in the desired property due to differences in the type of bonding, ionic versus covalent. For example, to synthesize a pyrochlore that has a structure compatible with the incorporation of Pu, one could choose a combination of A-site cations to yield an average A-site ionic radius equal to that of Pu. However, should this structure become disordered, the presence of the Pu would

result in an unknown response with respect to the stability of the structure. In the case of pyrochlore compositions which are ionic conductors, the Frenkel-pair defect formation energies, which largely control the oxygen migration energy, can vary significantly both due to the radii of the cationic species, as well as the details of the bonding between the B-site cation and oxygen. Based on these conclusions, we would predict that pyrochlore compositions with a variety of bond types on the B-site should show further surprising results with respect to chemically induced ionic conductivity or radiation "tolerance" changes. $A_2Ru_2O_7$ and $A_2Pb_2O_7$ pyrochlores and solid solutions with other tetravalent cations on the B site specifically might also show surprising behavior. As Ru and Pb both are rather electronegative (2.2 and 2.33, respectively) and would be expected to form strongly covalent bonds with oxygen, we anticipate that these compositions will be more resistant to defect formation than more ionically bonded solid solutions of the same mean cation radius.

ACKNOWLEDGMENTS

This work was supported by the National Science Foundation under Grant No. EAR-0230154 (L.S.), and the Office of Basic Energy Sciences, U.S. DOE, Grant No. DE-FG02-97ER45656 (R.C.E.).

*Author to whom correspondence should be addressed. Email address: wpanero@umich.edu

[1] B. J. Wuensch, K. W. Eberman, C. Heremans, E. M. Ku, P. Onnerud, E. M. E. Yeo, S. M. Haile, J. K. Stalick, and J. D. Jorgensen, Solid State Ionics **129**, 111 (2000).
[2] J. Yamaura, Y. Muraoka, F. Sakai, and Z. Hiroi J. Phys. Chem. Solids **63**, 1027 (2002).
[3] J. K. Park, C. H. Kim, K. J. Choi, H. D. Park, and S. Y. Choi, J. Mater. Res. **16**, 2568 (2001).
[4] M. J. P. Gingras, B. C. den Hertog, M. Faucher, J. S. Gardner, S. R. Dunsiger, L. J. Chang, B. D. Gaulin, N. P. Raju, and J. E. Greedan, Phys. Rev. B **62**, 6496 (2000).
[5] A. E. Ringwood, S. Kesson, N. G. Ware, and W. Hibberson, A. Major, Nature (London) **278**, 219 (1979).
[6] R. C. Ewing, W. J. Weber, and J. Lian, J. Appl. Phys. **95**, 5949 (2004).
[7] S. X. Wang, L. M. Wang, R. C. Ewing, and K. V. G. Kutty, Mater. Res. Soc. Symp. Proc. **540**, 355 (1999).
[8] A. A. Digeos, J. A. Valdez, K. E. Sickafus, S. Atiq, R. W. Grimes, and A. R. Boccaccini, J. Mater. Sci. **38**, 1597 (2003).
[9] S. X. Wang, B. D. Begg, L. M. Wang, R. C. Ewing, W. J. Weber, and K. V. G. Kutty, J. Mater. Res. **14**, 4470 (1999).
[10] J. Lian, L. M. Wang, J. Chen, K. Sun, R. C. Ewing, J. M. Farmer, and L. A. Boatner, Acta Mater. **51**, 1493 (2003).
[11] N. J. Hess, B. D. Begg, S. D. Conradson, D. E. McCready, R. P. Gassman, and W. J. Weber, J. Phys. Chem. B **106**, 4663 (2002).
[12] S. Kramer, M. Spears, and H. L. Tuller, Solid State Ionics **72**, 59 (1994).
[13] H. Takamura and H. L. Tuller, Solid State Ionics **134**, 67 (2000).
[14] J. Lian, J. Chen, L. M. Wang, R. C. Ewing, J. M. Farmer, L. A. Boatner, and K. B. Helean, Phys. Rev. B **68**, 134107 (2003).
[15] B. D. Begg, W. J. Weber, R. Devanathan, and J. P. Icenhower, Ceram. Trans. **107**, 553 (2000).
[16] B. D. Begg, N. J. Hess, D. E. McCready, S. Thevuthasan, and W. J. Weber, J. Nucl. Mater. **289**, 188 (2001).
[17] K. B. Helean, S. V. Ushakov, C. E. Brown, A. Navrotsky, J. Lian, R. C. Ewing, J. M. Farmer, and L. A. Boatner, J. Solid State Chem. **177**, 1858 (2004).
[18] M. Pirzada, R. W. Grimes, L. Minervini, J. F. Maguire, and K. E. Sickafus, Solid State Ionics **140**, 201 (2001).
[19] K. E. Sickafus, L. Minervini, R. W. Grimes, J. A. Valdez, M. Ishimaru, F. Li, K. J. McClellan, and T. Hartmann, Science **289**, 748 (2000).
[20] L. Minervini, R. W. Grimes, Y. Tabira, R. L. Withers, and K. E. Sickafus, Philos. Mag. A **82**, 123 (2002).
[21] A. Chartier, C. Meis, W. J. Weber, and L. R. Corrales, Phys. Rev. B **65**, 134116 (2002).
[22] P. J. Wilde and C. R. A. Catlow, Solid State Ionics **112**, 173 (1998).
[23] R. E. Williford, W. J. Weber, R. Devanathan, and J. D. Gale, J. Electroceram. **3**, 409 (1999).
[24] R. D. Shannon and C. T. Prewitt, Acta Crystallogr., Sect. B: Struct. Crystallogr. Cryst. Chem. **B25**, 925 (1969).
[25] B. C. Chakoumakos, J. Solid State Chem. **53**, 120 (1984).
[26] C. Heremans, B. J. Wuensch, J. K. Stalick, and E. Prince, J. Solid State Chem. **117**, 108 (1995).
[27] M. Glerup, O. F. Nielsen, and F. W. Poulsen, J. Solid State Chem. **160**, 25 (2001).
[28] M. T. Vandenborre, E. Husson, J. P. Chatry, and D. Michel, J. Raman Spectrosc. **14**, 63 (1983).
[29] D. L. Rousseau, R. P. Bauman, and S. P. S. Porto, J. Raman Spectrosc. **10**, 253 (1981).
[30] K. B. Helean, B. D. Begg, A. Navrotsky, B. Ebbinghaus, W. J. Weber, and R. C. Ewing, Mater. Res. Soc. Symp. Proc. **663**, 691 (2001).
[31] G. Kresse, J. Hafner, and R. J. Needs, J. Phys.: Condens. Matter **4**, 7461 (1992).
[32] G. Kresse and D. Joubert, Phys. Rev. B **59**, 1758 (1999).
[33] G. Kresse and J. Hafner, Phys. Rev. B **47**, 558 (1993).
[34] G. Kresse and J. Furthmüller, Comput. Mater. Sci. **6**, 15 (1996).
[35] G. Kresse and J. Furthmüller, Phys. Rev. B **54**, 11 (1996).
[36] J. Aidun, M. S. T. Bukowinski, and M. Ross, Phys. Rev. B **29**, 2611 (1984).
[37] F. A. Kröger and H. J. Vink, J. Phys. Chem. Solids **5**, 208 (1958).
[38] W. R. Panero and R. C. Ewing (unpublished).
[39] O. L. Anderson and J. E. Nafe, J. Geophys. Res. **70**, 3951 (1965).
[40] Y. Tabira, R. L. Withers, L. Minervini, and R. W. Grimes, J. Solid State Chem. **153**, 16 (2000).
[41] B. Kiefer, L. Stixrude, J. Hafner, and G. Kresse, Am. Mineral. **86**, 1387 (2001).
[42] H. M. Naguib and R. Kelly, Radiat. Eff. **25**, 1 (1975).
[43] J. Lian, L. M. Wang, R. C. Ewing, and B. J. Kennedy (unpublished).